Materials Science Forum
ISSN: 1662-9752, Vol. 1185, pp 41-53
doi:10.4028/p-Kld5TA

Submitted: 2026-01-13
Revised: 2026-02-15
Accepted: 2026-02-23
Online: 2026-04-15

Micro Friction Stir Spot Welding for Copper Current Collector Applications – An Experimental Study

Schwichtenberg Nik[1,a*], Tesch Markus[1,b], Sigl Martina E.[1,c], Goeldner Moritz[1,d] and Zaeh Michael F.[1,e]

[1]Institute for Machine Tools and Industrial Management (iwb), TUM School of Engineering and Design, Technical University of Munich, Boltzmannstrasse 15, Garching, Germany

[a*]nik.schwichtenberg@iwb.tum.de, [b]markus.tesch@iwb.tum.de, [c]martina.sigl@iwb.tum.de, [d]moritz.goeldner@iwb.tum.de, [e]michael.zaeh@iwb.tum.de

[*]corresponding author

Keywords: micro friction stir spot welding, current collectors, busbars, electrical contacting, printed circuit boards.

Abstract. The growing demand for advanced energy storage systems, power electronics, and electrical interconnections requires joining processes that ensure both electrical conductivity and mechanical stability. Applications such as battery cell-internal contacts, flexible busbar connections, and printed circuit board (PCB) conductor interfaces impose strict requirements on material combinations, layer thicknesses, and thermal management, which influence the suitability of the joining processes. Micro friction stir spot welding (µFSSW) offers advantages through its low thermal impact as well as its high process robustness and through the bonding of the joining partners in solid state. In the studies presented in this article, transferable simplified specimens were designed to systematically evaluate process parameters for different applications of µFSSW. The feasibility of a full contact using µFSSW was assessed through electrical resistance measurements, mechanical shear testing, and morphological examinations of the weld zone, as well as axial force measurements during the welding process. The results demonstrate the suitability of µFSSW for copper-based current collector foils in cell-internal contacts, busbar interconnections, and PCB junctions, and they highlight key relationships between the process conditions and the electrical, mechanical, and structural performance. The study also highlights challenges and opportunities for a future industrial implementation.

Introduction

Electrical interconnections play a critical role in modern industrial systems, where reliability, low electrical resistance, and mechanical robustness must be ensured across increasingly diverse product portfolios. This is particularly evident in lithium-ion batteries for which performance demands have risen sharply due to the global push towards electrification and energy-dense storage systems. Higher energy densities require thinner current collector foils and more electrode layers, all of which increase the sensitivity of the contacting process to geometric variations [1, 2]. And the teardown studies of modern lithium-ion cells, including the Tesla 4680 and the BYD Blade formats, illustrate that the number of electrodes, foil thicknesses, and tab connection quality directly influence electrical losses and thermal behavior [3, 4]. These geometric variations necessitate contacting processes with a high robustness towards changing joining setups.

Busbar systems for power electronics and e-mobility have to meet the requirement of growing current levels by adjusting conductor cross-sections or by integrating multilayer copper stacks, which pose additional challenges for joining technologies [5, 6]. Laminated busbars and complex multilayer conductor systems necessitate joints with a low electrical resistance and negligible thermal distortion. PCB-based conductor interfaces introduce another challenge, as embedded and surface-mounted copper structures are highly sensitive to local heat input [7].

Established joining processes, such as ultrasonic welding, resistance spot welding, and laser beam welding are widely used but show significant limitations concerning these evolving requirements.

Ultrasonic welding is strongly affected by variations in stack thickness and foil count, which hinder energy coupling and lead to reduced weld uniformity [6]. Laser beam welding offers high precision but introduces steep thermal gradients, risking damage to sensitive battery and PCB substrates and causing inconsistent weld depths in multilayer copper stacks [8–11]. Resistance spot welding suffers from the high thermal conductivity of copper, which makes nugget formation difficult and increases the risk of expulsion or interfacial defects [12].

Micro friction stir spot welding (µFSSW) offers a solid-state, low-temperature alternative that directly addresses these challenges of changed joining partner geometries. In this work, the term micro friction stir spot welding refers to the application of friction stir spot welding to ultra-thin sheet and foil stacks with very low thermal mass. The designation “micro” therefore relates to the scale of the thermo-mechanical interaction zone and process conditions rather than to the absolute tool dimensions [13, 14]. As demonstrated by Sigl et al. [1], µFSSW enables robust joining of thin copper and aluminum current collector stacks while maintaining low contact resistance. Earlier work by Li et al. [15] showed that µFSSW leads to stable interconnections with limited thermal impact and favorable electrical behavior, making it well-suited for copper-based applications. Recent research emphasizes the remarkable robustness of the process against geometric variations, including changes in foil number, layer thickness, and stack composition. Tool geometry and process parameters influence hook formation, bond width, and static strength, but the process window remains highly tolerant [16–18]. For busbar and multilayer applications, friction-stir-based processes have been shown to achieve copper joints with refined microstructures and a predictable and enhanced conductivity behavior [19]. Given the limitations of conventional joining processes and the increasing geometric complexity of industrial applications, µFSSW provides a promising alternative for producing stable, reproducible, and electrically efficient joints. However, a systematic comparison across battery current collectors, busbars, and PCB interconnections has not yet been comprehensively addressed. This work therefore investigates the suitability of µFSSW across these three representative application classes, evaluates its feasibility using simplified application-specific geometries, and analyzes the influence of relevant process parameters. The study is structured into two consecutive experimental investigations.

In the first study, selected application-specific specimens were examined using simplified geometries that reflect the essential joint designs of the respective applications. This feasibility study aimed to achieve full penetration of the multilayer stacks and to identify characteristic effects arising from the different joint configurations and material arrangements.

Building on these results, a second study was conducted using derived analysis specimens that consolidate the characteristic contact features of the investigated applications into a unified geometry. This approach enables a reproducible and statistically meaningful evaluation with a focused assessment of electrical resistance and mechanical strength, providing a consistent basis for analyzing process–property relationships.

Specimen Concept

The three selected application cases share one common functional principle. In all configurations, multiple thin conductive elements must be reliably joined within a confined interface to form a low-resistance current collector. However, the geometric characteristics of the joining partners vary significantly across applications. Transferable specimen designs were therefore needed that fulfill both the functional requirements and the differing boundary conditions. For the feasibility study, simplified geometries were derived that represent the essential stack dimensions and joining zones of each application while eliminating construction-specific constraints. These simplified specimens enable a consistent assessment of µFSSW under comparable conditions.

Fig. 1 shows illustrations of the three applications. In lithium-ion battery pouch cells (a), thin copper or aluminum electrode foils are contacted to a metallic arrestor tab to form the internal current collector. Flexible busbars (b) conduct high currents between power-electronic subsystems using laminated copper or aluminum foils enclosed by thin forming sheets, combining a high current-carrying cross-sectional area with mechanical flexibility. PCB-based conductor interfaces (c) rely on

copper structures on or within FR4 substrates (common substrate material in printed circuit boards), either as surface-mounted foil stacks or as embedded copper baseplates.

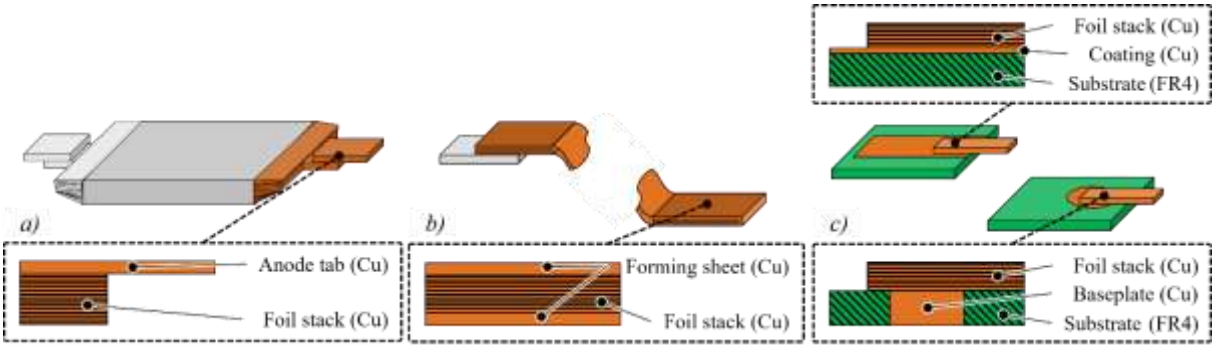

Fig. 1. Joining geometries of investigated current collector applications:
a) cell-internal contacts, b) flexible busbars,
c) PCB collector spots, coated (top) and embedded (buttom).

For the feasibility study, only copper-based joints were investigated. This avoided additional effects from dissimilar interfaces and enabled a clear assessment of µFSSW under controlled, comparable conditions. The selection of copper is justified, as it accounts for a substantial proportion of conductor applications in electrical systems [20]. The specimen configurations derived are presented in Table 1. The materials investigated include OF-Cu R200 and PHC SE-Cu R360, which are widely used in electronic components due to their high electrical conductivity, as well as FR4.

Table 1. Materials and configurations of the application specimens.

Cell-internal contact					**PCB collector spot (coated)**		
	Qty	Material	Size in mm		Qty	Material	Size in mm
Arrestor	1	OF-Cu R200	40×20×0.2	Cover sheet	1	OF-Cu R200	15×20×0.2
Foil stack	11	PHC SE-Cu R360	40×20×0.01	Foil stack	10	PHC SE-Cu R360	0.01
Bottom sheet	1	OF-Cu R200	20×20×0.2	PCB	1 1	FR4 ED-Cu	30×30×0.8 30×30×0.035
Flexible busbar					**PCB collector spot (embedded)**		
	Qty	Material	Size in mm		Qty	Material	Size in mm
Forming sheet	1	OF-Cu R200	40×20×0.2	Cover sheet	1	OF-Cu R200	15×20×0.2
Foil stack	10	PHC SE-Cu R360	40×20×0.01	Foil stack	10	PHC SE-Cu R360	40×20×0.01
Forming sheet	1	OF-Cu R200	40×20×0.2	PCB	1 1	FR4 OF-Cu R200	30×30×0.5 ø10×0.5

Based on the simplified geometries used in the feasibility study, a universal analysis geometry was derived to enable reproducible and comparable measurements for electrical and mechanical testing across all application cases. This geometry represents the essential functional elements of the multilayer conductor joints while standardizing overlap width, foil stack composition, and clamping conditions. As shown in Fig. 2, the analysis specimen provides a controlled experimental environment for evaluating mechanical properties such as shear strength as well as electrical characteristics like contact resistance. By eliminating application-specific geometric variability, this specimen allows the influence of process parameters and of the weld morphology on the joint performance to be assessed consistently and with high statistical reliability.

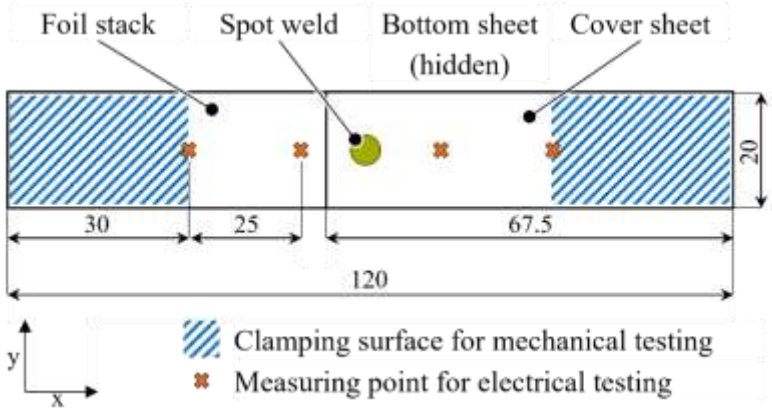

Fig. 2. Schematic illustration and dimensions of the analysis geometry.

In Table 2, the materials and specimen configurations used in study 2 are summarized. The number of foils in the stack was variably scalable, which allowed for different conductor cross-sections. A bottom sheet was included only for smaller stacks to prevent unintentional welding to the clamping fixture. This adaptable setup ensured consistent testing across a wide range of multilayer configurations.

Table 2. Material and configuration of the analysis specimens.

	Qty	Material	Size in mm
Cover sheet	1	OF-Cu R200	67.5×20×0.2
Foil stack	11	PHC SE-Cu R360	67.5×20×0.01
Bottom sheet	1	OF-Cu R200	15×20×0.2

Experimental Setup

The welding experiments were conducted in position-controlled mode on a four-axis horizontal milling machine (MCH 250, Gebr. Heller Maschinenfabrik GmbH, Nuertingen, Germany), which had been adapted for friction stir welding. The µFSSW tool was manufactured from hardened X38CrMoV5-1 tool steel and coated with a TiBZr to improve wear resistance and thermal stability. The detailed tool geometry and dimensions are shown in Fig. 3.

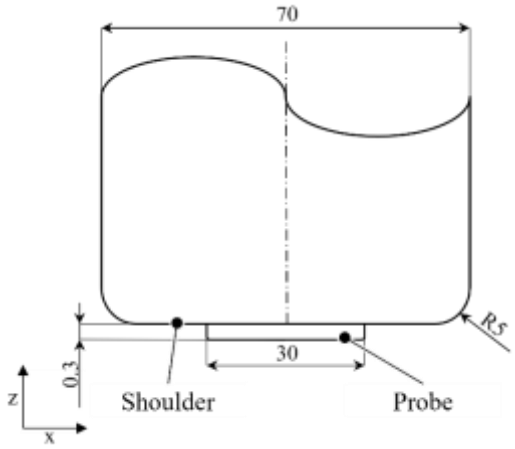

Fig. 3. µFSSW tool geometry.

For the feasibility study, representative application specimens were welded using the parameter sets listed in Table 3 in total 48 welding specimens. They were chosen based on prior experimental results. The objective of study 1 was to determine parameter combinations that achieve full penetration and stable weld formation for the three application-specific stack configurations. Study 1 was designed

as a feasibility and transferability investigation rather than a parameter optimization. A limited number of representative parameter sets was therefore applied across all application geometries to identify geometry-dependent effects in weld formation.

Table 3. Process parameters for the application trials (study 1).

Parameter Configuration (PC)	Rotational speed n in min^{-1}	Plunge depth z_p in mm	Plunge speed v_p in mm/min	Dwell time t_d in s
PC 1	2900	0.05	20	0.25
PC 2	2900	0.05	20	0.5
PC 3	2900	0.75	20	0.25
PC 4	3400	0.05	20	0.25

Based on these results, a study 2 was conducted using the standardized analysis specimen and applying a full factorial experimental design. The variations in the parameters investigated are summarized in Table 4 with in total 384 welding specimens. Each parameter combination was produced twice. The focus was on covering a wide parameter space and identifying general trends rather than determining the variance at individual parameter points. The plunge depth is defined relative to the shoulder surface.

Table 4. Process parameters for the parameter study (study 2).

Rotational speed n in min^{-1}	Plunge depth z_p in mm	Plunge speed v_p in mm/min	Dwell time t_d in s
2900	0.00	20	0.1
3400	0.025	30	0.15
3900	0.05	40	0.25
4400	0.075		0.5

During all welding trials, the process forces and the moments were recorded using a SPIKE mobile HSK-A63 HD20 110 A sensor (Pro-Micron GmbH, Kaufbeuren, Germany), which was mounted between the spindle and the tool. This system enables real-time acquisition of axial forces as well as bending and torsional moments, providing additional insights into material flow and weld formation. A subset of welded specimens was prepared for metallographic cross-section analysis and examined using a Keyence VHX-7000 digital microscope to evaluate weld morphology, bonding interfaces, and the occurrence of welding defects. Mechanical characterization was conducted as lap-shear testing based on DIN 50154 [21] on a Zwick Roell Z050 testing machine (ZwickRoell GmbH & Co. KG, Ulm, Germany). The electrical performance was evaluated using a four-point resistance measurement setup (see Fig. 2) based on the methodology described by Grabmann et al. [22]. Table 5 lists the applied measurement parameters.

Table 5. Measurement parameters for mechanical and electrical testing.

Tensile testing		**Resistance testing**	
Parameter	Value	Parameter	Value
Test speed v_p in mm/min	2	Test current I_0 in A	10
Clamping distance L_0 in mm	60	Voltage U_0 in V	5
Preload F_0 in N	1	Ref. temperature t_{ref} in °C	22

This integrated experimental framework enabled a reproducible assessment of the weld formation, the mechanical strength, the electrical resistance, and the process behavior for all investigated µFSSW conditions.

Results of the Application Trials (Study 1)

In the application experiments, micro-friction stir spot welds were successfully manufactured for all investigated specimen configurations. Only in one case, namely the PCB collector spot (coated) specimen (PC 4), delamination was observed. This might have occurred due to the high rotational speed. Fig. 4 shows the corresponding cross-sectional images of the welded joints. The welds exhibit characteristic features typical for the µFSSW process, including the distinct tool imprint and the associated local reduction in specimen thickness, accompanied by material displacement into the surrounding regions. Within the cover sheet, this displacement leads to a localized deformation that forms a void region and induces a hooking effect into the foil stack underneath. These structural characteristics provide essential insights into the material flow and joint formation mechanisms governing the resulting weld quality.

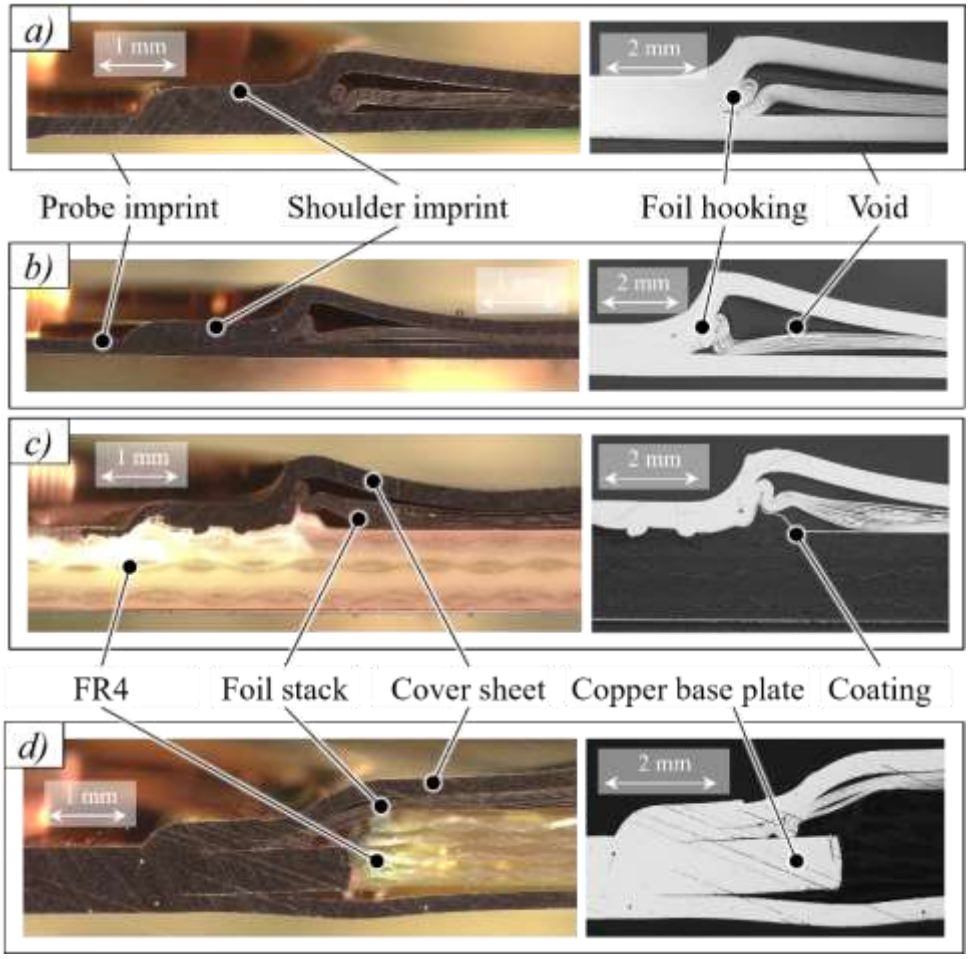

Fig. 4. Cross-sections of the application trials of study 1 (PC 3): a) cell-internal contact, b) flexible busbar, c) PCB collector spot (coated) and d) PCB collector spot (embedded).

Several irregularities were observed in the weld perimeter and surrounding material zones. Examples are illustrated in Fig 5. These irregularities include the formation of flash around the shoulder contact area, local delamination within the laminated structure, and notches resulting from partial bonding at the outer edge of the weld. While no fractures or breakages of the foils were detected in the examined specimens, such defects cannot be fully ruled out, particularly in regions experiencing pronounced deformation. Likewise, the generation or embedding of micro-debris caused by abrasive interactions during the process may occur, although no distinct particles were identified in the present metallographic sections. These observations highlight the complex interaction between tool penetration, material flow, and layered composite response under the thermomechanical loading conditions characteristic of µFSSW.

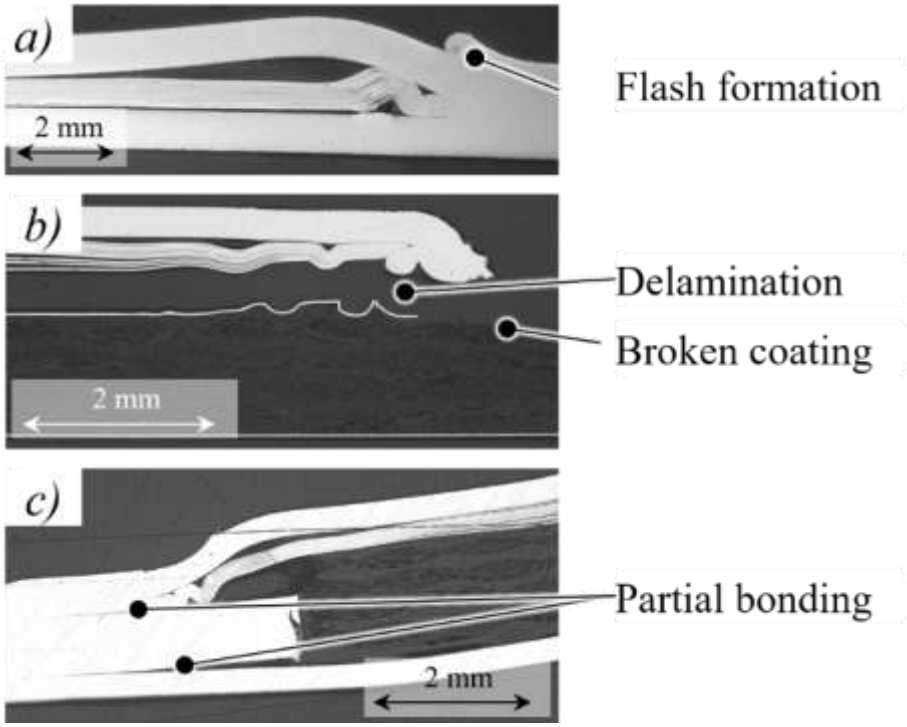

Fig. 5. Cross-sections of irregularities of the application trials (PC 4):
a) cell-internal contact, b) PCB collector spot (coated) and c) PCB collector spot (embedded).

The evaluation of the axial force signals for the different application specimens reveals that all copper-based specimen configurations exhibit a comparable force progression (see Fig. 6) during the µFSSW process. Such force curves can be clearly associated with the fundamental process phases, namely the plunge phase during which the tool penetrates and plasticizes the material, the dwell phase during which frictional heating and material consolidation dominate, and the retract phase in which the tool is withdrawn and the joint solidifies, as presented in the figure. For the investigated applications cell-internal contact, flexible busbar, and PCB collector spot (embedded), the extracted curves display nearly identical trends, indicating a high level of repeatability and demonstrating that the axial force response is predominantly influenced by the underlying thermomechanical process rather than by moderate geometric or thickness variations between the specimen designs. In contrast, the PCB collector spot (coated) application exhibits a noticeably increased maximum axial force. This behavior can be attributed to the reduced deformation capability of the substrate plate.

Beyond the overall curve progression, characteristic points relevant for process interpretation can be identified, including the initial force rise during the plunge phase, the force stabilization and material consolidation during the dwell phase, and the distinct drop associated with the retract phase. Only the force discontinuity that typically occurs when the tool shoulder reaches the material, often visible as a sharp force jump, was not always clearly pronounced. This variation may result from local surface conditions or slight differences in contact mechanics; however, it does not impede the overall comparability of the curves.

A deviation from this consistent behavior is observed for the PCB collector spot-coated application. In contrast to the purely copper-based specimens, this configuration incorporates an FR4 substrate, whose mechanical stiffness, thermal conductivity, and deformation behavior differ considerably from those of metallic substrates. These material differences may dampen or distort segments of the axial force curve, resulting in a reduced transferability of the characteristic force progression. This effect was considered during the design of the analysis geometry to ensure that material-specific deviations do not compromise the identification of general process features.

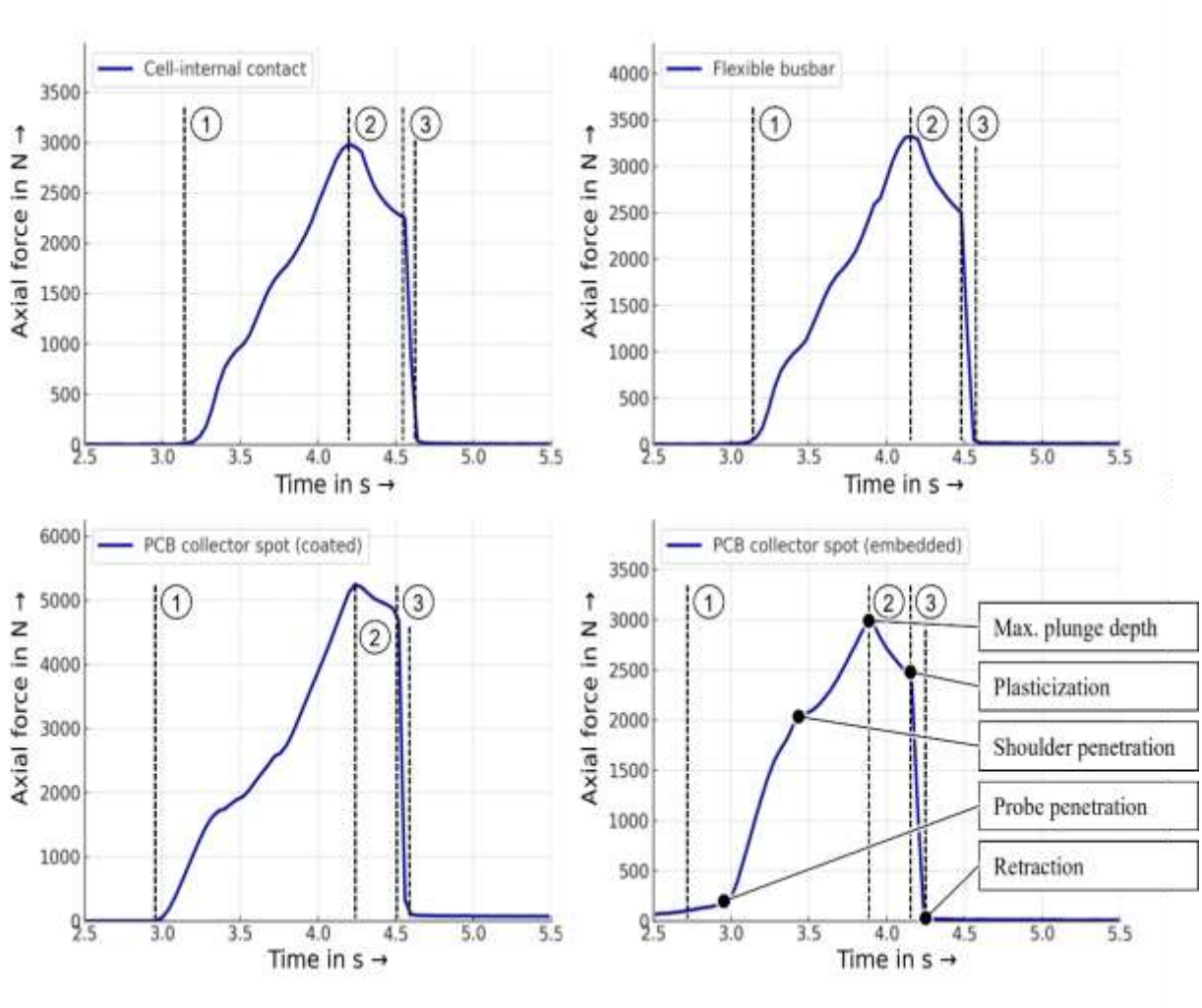

Fig. 6. Axial force curves of the application trials (PC 3):
1: plunge phase, 2: dwell phase, 3: retract phase.

Results of the Parameter Study (Study 2)

To evaluate the influence of the main process parameters on the resulting quality characteristics, a correlation analysis was conducted using both the Pearson correlation coefficient and the Spearman rank correlation. The application of these two methods enables the detection of different types of statistical relationships. The Pearson correlation coefficient describes linear dependencies between metric variables and assumes an approximately linear relationship or normally distributed data [23]. Since thermo-mechanical joining processes frequently exhibit parameter regions with near-linear scaling behavior, Pearson is well suited to identify such relationships. In contrast, the Spearman correlation is based on ranked data and captures monotonic, but not necessarily linear relationships, making it more robust against outliers and able to represent nonlinear trends [24]. This is particularly advantageous because joining processes often exhibit saturation effects or threshold behaviors. The combined use of both approaches therefore provides a comprehensive view of the underlying parameter-response structure (see Table 6).

Table 6. Correlation matrix according to Pearson and Spearman for the process parameters and the electrical and mechanical properties.

	Pearson correlation/ p-value		**Spearman correlation/ p-value**	
Process parameter	El. resistance	Tensile force	El. resistance	Tensile force
Plunge depth	-0.68/ 5.1×10^{-53}	0.57/ 1.6×10^{-33}	-0.69/ 5.4×10^{-56}	0.58/ 7.9×10^{-35}
Rotational speed	-0.31/ 1.3×10^{-9}	0.37/ 1.2×10^{-13}	-0.30/ 3.0×10^{-9}	0.38/ 6.3×10^{-14}
Dwell time	-0.22/ 1.7×10^{-5}	0.10/ 0.065	-0.23/ 2.3×10^{-5}	0.13/ 0.023
Plunge speed	0.07/ 0.13	-0.18/ 3.9×10^{-4}	0.07/ 0.13	-0.18/ 5.1×10^{-4}

Both correlation methods reveal consistent trends, confirming that plunge depth and rotational speed are the primary factors influencing electrical resistance and tensile strength. Plunge depth exhibits the highest absolute correlation coefficients, showing a negative relationship with electrical resistance and a positive relationship with tensile strength. This is consistent with the physical expectation that deeper tool engagement promotes enhanced plastic deformation and improved bonding conditions, thereby facilitating effective metallic contact formation.

Rotational speed shows moderate but stable correlations with both target metrics, reflecting its role in frictional heat generation, material plasticization, and joint consolidation. From a statistical perspective, the associated correlation coefficients are accompanied by low p-values, indicating that these relationships are unlikely to arise by chance. However, statistical significance is interpreted in conjunction with effect size and physical plausibility rather than as a binary criterion.

The dwell time displays lower correlation coefficients than the plunge depth but reaches values comparable to those of the rotational speed for the tensile strength. Although the corresponding p-values indicate only marginal statistical significance, this suggests that the dwell time contributes measurably to a process refinement rather than acting as a dominant control parameter within the investigated process window.

In contrast, the plunge speed shows only very weak correlations with the electrical resistance. While these correlations may reach statistical significance due to the relatively large sample size, their low effect magnitude indicates limited practical relevance. Consequently, the influence of the plunge speed on the electrical performance is considered secondary.

Based on these findings, the subsequent graphical evaluation focuses on plunge depth and rotational speed as the primary variables governing the joining outcome. These parameters exhibit the strongest and most physically meaningful relationships with the quality metrics and therefore provide a robust basis for analyzing process–property interactions. This rationale underpins the decision to focus further investigations on these two factors.

The boxplot representation (median, upper and lower quantile) of the electrical resistance and mechanical tensile strength for the selected process parameter combinations provides a clear visual indication on how the plunge depth and the rotational speed influence the joining performance (see Fig. 7). As observed, increasing both plunge depth and rotational speed leads to a systematic improvement in joint quality, reflected by a decrease in electrical resistance and an increase in tensile strength. These trends are consistent with the outcomes of the correlation analysis, which identified both parameters as the primary drivers of the process behavior due to their strong monotonic and linear relationships with the target metrics.

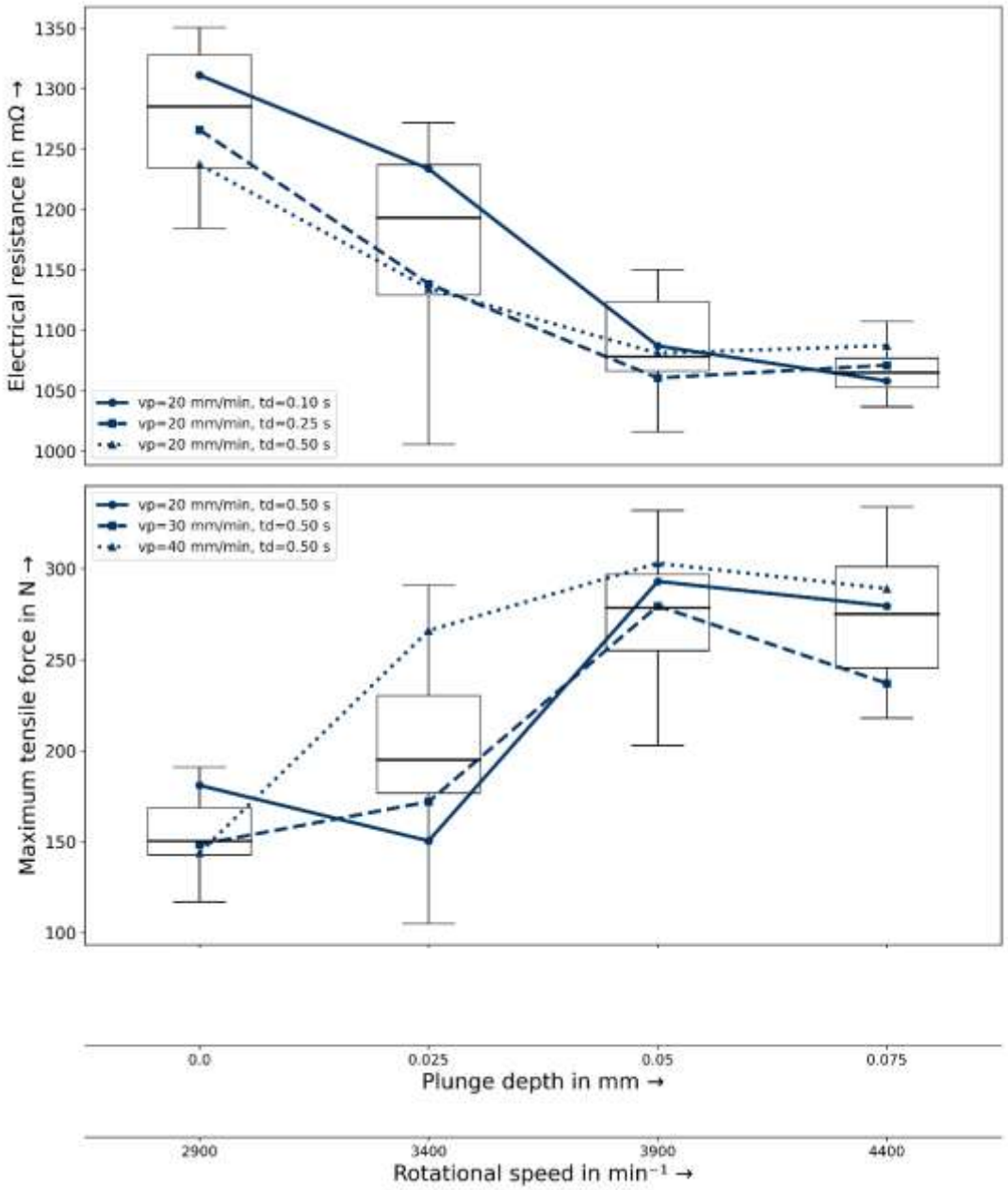

Fig. 7. Boxplots of electrical resistance (top) and tensile strength (bottom) for different combinations of plunge depth and rotational speed.

A notable feature in the graphical evaluation is the distinctly larger spread of values associated with the process parameter combination of a plunge depth of 0.025 mm and a rotational speed of 3400 min^{-1}. For this specification, a noticeable increase in scatter is observed in both electrical resistance and mechanical tensile strength. The evaluation across the remaining process parameters, dwell time and plunge speed, reveals that certain parameter settings, especially those involving higher plunge speeds and longer dwell times, lead to substantial fluctuations. In these cases, electrical resistance can vary by more than 100 mΩ, while tensile strength differences exceed 100 N. This pronounced variance indicates that the 0.025 mm/3400 min^{-1} combination is particularly sensitive to changes in the additional parameters and results in a higher process variability in the joining performance.

In contrast, the parameter sets associated with larger plunge depths and higher rotational speeds show significantly narrower distributions in both resistance and tensile strength. This reduced variance suggests more stable thermomechanical conditions, improved material consolidation, and overall more reliable process outcomes.

Overall, the combined interpretation of the boxplots and the correlation results highlight the central role of plunge depth and rotational speed in determining both the absolute quality values and the

consistency of the joining process. These findings confirm the suitability of focusing subsequent investigations on these two dominant parameters.

Discussion of study 1: Application-specific feasibility and joint robustness

The results of the first study demonstrate the suitability and robustness of µFSSW across the investigated application-specific joint designs. Full penetration of the multilayer stacks was achieved for all current collector applications using an identical tool geometry and a common set of process parameters, indicating a resilience with respect to joint design and stack configuration.
Metallographic cross-sections reveal characteristic features of µFSSW, including tool imprint formation, local thinning, and material displacement around the weld zone, which are consistently observed across all applications. These findings indicate stable material flow conditions and underline the suitability of µFSSW for heterogeneous copper-based current collector designs.
A delamination was observed in the coated PCB collector configuration. However, it cannot be conclusively determined whether this effect originated during welding or occurred during specimen preparation. While this observation suggests a potential sensitivity of FR4-based substrates, it does not allow for an unambiguous attribution to the joining process itself.

Discussion of study 2: Parameter influence and process–property relationships

The second study confirms that plunge depth and rotational speed are the dominant process parameters governing the joint quality in µFSSW, consistent with established thermomechanical joining principles [1, 2]. Increased plunge depth enhances material engagement and bonding, while higher rotational speed promotes frictional heating and plasticization, resulting in reduced electrical resistance and increased tensile strength.
Dwell time and plunge speed exhibit lower correlation coefficients and therefore act mainly as tuning parameters within the investigated process window. Although their influence is statistically detectable, their effect magnitude remains limited compared to the dominant parameters. Axial force analysis further corroborates these findings. Comparable force–time signatures for copper-based specimens indicate stable process mechanics.

Conclusion and Outlook

This study demonstrates that µFSSW enables the reliable formation of fully consolidated joints across various copper-based current collectors, with plunge depth and rotational speed identified as the dominant parameters influencing electrical and mechanical performance. The combination of correlation analysis, metallographic examination, and axial force evaluation reveals consistent process behavior among the copper-based applications, while deviations observed in the coated PCB configuration highlight the role of substrate-specific thermo-mechanical properties.
Future work should focus on a more detailed assessment of deformation phenomena, including the extent of thinning, surface indentation and subsurface material displacement, in order to better understand their relevance for electrical and mechanical functionality. Furthermore, investigating internal irregularities, such as voids or delamination fronts, will be essential for establishing robust quality criteria. In addition, the influences of varying foil thicknesses and stack heights are to be investigated.
Acknowledgements. This work was funded by the German Federal Ministry of Research, Technology, and Space (BMBFTR) under grant 03XP0545. We would like to thank the BMBFTR and the project management organization Julich (PTJ) for their support. We thank Jana Hauptmann for the sample preparation und Eren Günal for assisting during the welding experiments.

References

[1] Sigl, M.E., Grabmann, S., Kick, L.F., Zens, A., Hartl, R., Zaeh, M.F., Cell-Internal Contacting of Prismatic Lithium-Ion Batteries Using Micro-Friction Stir Spot Welding, Batteries 8 (2022) 174.

[2] Pettinger, K-H., Kampker, A., Hohenthanner, C-R., Deutskens, C., Heimes, H., vom Hemdt, A., Lithium-ion cell and battery production processes, in: Korthauer, R. (Ed.), Lithium-Ion Batteries: Basics and Applications, Springer, Berlin, Heidelberg, 2018, pp. 211–226.

[3] Ank, M., Sommer, A., Abo Gamra, K., Hensel, J., Frieges, M., Schneider, J., Reinhart, G., Lithium-Ion Cells in Automotive Applications: Tesla 4680 Cylindrical Cell Teardown and Characterization, J. Electrochem. Soc. 170 (2023) 120536.

[4] Gorsch, J., Schneiders, J., Frieges, M., Ank, M., Sommer, A., Reinhart, G., Contrasting a BYD Blade prismatic cell and Tesla 4680 cylindrical cell, Cell Reports Phys. Sci. 6 (2025) 102453.

[5] Singh, P.B.T., Bobba, P.B., Suresh, K., Varghese, B.J., Extensive review on laminated bus bar for low and high power applications, E3S Web Conf. 87 (2019) 01009.

[6] Sampaio, R.F.V., Zwicker, M.F.R., Pragana, J.P.M., Pinto, A.M.P., Silva, F.J.G, Busbars for e-mobility: State-of-the-Art Review and a New Joining by Forming Technology, in: Davim, J.P. (Ed.), Mechanical and Industrial Engineering, Springer, Cham, 2022, pp. 111–141.

[7] Jillek, W., Yung, W.K.C., Embedded components in printed circuit boards: a processing technology review, Int. J. Adv. Manuf. Technol. 25 (2005) pp. 350–360.

[8] Grabmann, S., Kriegler, J., Harst, F., Günter, F.J., Zaeh, M.F., Laser welding of current collector foil stacks in battery production, Int. J. Adv. Manuf. Technol. 118 (2022) pp. 2571–2586.

[9] Grabmann, S., Mayr, L., Kick, M.K., Zaeh, M.F., Enhancing laser-based contacting of aluminum current collector foils, Procedia CIRP 111 (2022) pp. 778–783.

[10] Grabmann, S., Tomcic, L., Zaeh, M.F., Laser beam welding of copper foil stacks using a green high-power disk laser, Procedia CIRP 94 (2020) pp. 582–586.

[11] Rinker, T.J., Pour, M.M., Wen, W., Katayama, S., Kawahito, Y., Investigating the Welding Limit of Copper Foils to a Tab for Battery Applications with a Green Laser, Journal of Materials and Performance 34 (2025) pp. 1-11.

[12] Wei, P.S., Wu, T.H., Electrical contact resistance effect on resistance spot welding, Int. J. Heat Mass Transf. 55 (2012) pp. 3316–3324.

[13] Sen, M., Shankar, S., Chattopadhyaya, S., Micro-friction stir welding (μFSW) – A review, Materials Today: Proceedings 27 (2020), pp. 2469-2473.

[14] Kumar Rajak, D., Pagar, D. D., Menezes, P. L., Eyvazian, A., Friction-based welding processes: friction welding and friction stir welding. Journal of Adhesion Science and Technology 34 (2020), pp. 2613–2637.

[15] Li, M., Zhang, C., Wang, D., Chen, G., Gao, Z., Friction Stir Spot Welding of Aluminum and Copper: A Review, Materials 13 (2019) 156.

[16] Amat, M.A., Andhika, I.D.G.R., Pratama, F.I., Kiswanto, G., Baskoro, A.S., The effects of tool geometry on static strength and failure mode in μFSSW, The International Journal of Advanced Manufacturing Technology 135 (2024) pp. 2697–2715.

[17] Tozaki, Y., Uematsu, Y., Tokaji, K., Effect of tool geometry on static strength in friction stir spot welded aluminium alloys, Int. J. Mach. Tools Manuf. 47 (2007) pp. 2230–2236.

[18] Labus Zlatanovic, D., Balos, S., Bergmann, J.P., Zerjav, G., Stamenkovic, D., Influence of tool geometry and parameters on FSSW of multiple ultrathin sheets, Materials 14 (2021) 1157.

[19] Li, Z., Deng, Y., Zeng, J., Liu, C., Wang, Y., Achievement of defect-free multilayer copper flexible connections by FSW, Welding in the World 68 (2024) pp. 1747–1756.

[20] International Copper Association (ICA), Annual Report 2022, International Copper Association, 2022.

[21] DIN 50154:2019-09, Tensile test on foils and strips of aluminum and aluminum wrought alloys with a nominal thickness less than 0.200 mm.

[22] Grabmann, S., Bernauer, C., Wach, L., Leeb, M., Zaeh, M.F., A method for the reproducible and accurate determination of electrical resistances on multi-layer joint in lithium-ion batteries. Applied Energy 349 (2023) S. 121613.

[23] Rodgers, J.L., Nicewander, W.A., Thirteen ways to look at the correlation coefficient, The American Statistician 42 (1988) pp. 59–66.

[24] Hauke, J., Kossowski, T., Comparison of values of Pearson's and Spearman's correlation coefficients on the same sets of data, Quaestiones Geographicae 30 (2011) pp. 87–93.